Detailed stability map and bistability investigation for injection-locked Fabry-Perot semiconductor lasers

M. M. Krstić,[1] M. L. Mašanović,[2] J. V. Crnjanski[1], L. A. Johansson,[2] L. A. Coldren,[2] and D. M. Gvozdić[1]
[1]*School of Electrical Engineering, University of Belgrade, Serbia*
[2]*ECE Department,University of California, Santa Barbara, CA 93106, USA*

Abstract: Novel, complex, multi-valued locking range and stability map are obtained for injection locked F-P lasers through inclusion, for the first time, of all supported modes. Predicted slave laser bi-stability is explained and experimentally confirmed.

The stable locking regime of an injection-locked laser is usually characterized by a stability map. This map is represented by a set of ordered pairs comprising angular frequency detuning $\Delta\omega$ between the master and the slave laser signal frequencies, and injection power ratio r (i.e. the ratio of the photon density S_{inj} injected into the slave laser and the photon density S_m of the injection-locked mode of the slave laser) for which the slave laser is stably locked to the master laser, Fig. 1. The stability map has previously been thought to be a single-valued function between $\Delta\omega$ and r [1-5]. In this work, we show that taking into account all unlocked modes in the slave laser operation analysis significantly impacts the locking range and provides multiplicity of the stability map. We then verify our theoretical findings by conducting an experiment which is in qualitative agreement with our theory. A key novelty here is that in the prior work on the analysis of the stability maps [2, 3], the unlocked slave laser modes have not been taken into account, although it was suggested that the unlocked modes be taken into account in the case of their collateral excitation during the injection locking or to account for gain suppression effects [1, 4].

As our theoretical analysis basis, we use a set of multimode rate equations describing the dynamics of injection-locked slave laser [5,6]. In our analysis, all photon densities are at least two orders of magnitude smaller than those necessary to trigger the mechanism of nonlinear gain suppression. For given values of $\Delta\omega$ and r in the locking range, this system of equations can have up to three steady-state solutions for carrier concentration n: basic solution n_L, which always exists, and two other solutions n_H and n_M, which can appear for certain ranges of negative $\Delta\omega$. Since the range in which n_M appears is extremely narrow [6], this solution will be excluded from further discussion. We focus on the basic solution n_L and study the stability map in the $\Delta\omega$-r space ($\Omega = 10^{10}$ rad/s corresponds to $\Delta f = 1.59$ GHz) for three different cases (Fig.1). Fig.1(a) shows the standard stability plot [2] obtained for the case of taking into account the injection-locked mode alone (in this case, the side mode m = -5 with a corresponding wavelength of 1555.7 nm). In the prior work [2], the unstable region was considered to be the whole region in which the slave laser doesn't lock to the master laser (Fig. 1(a)).

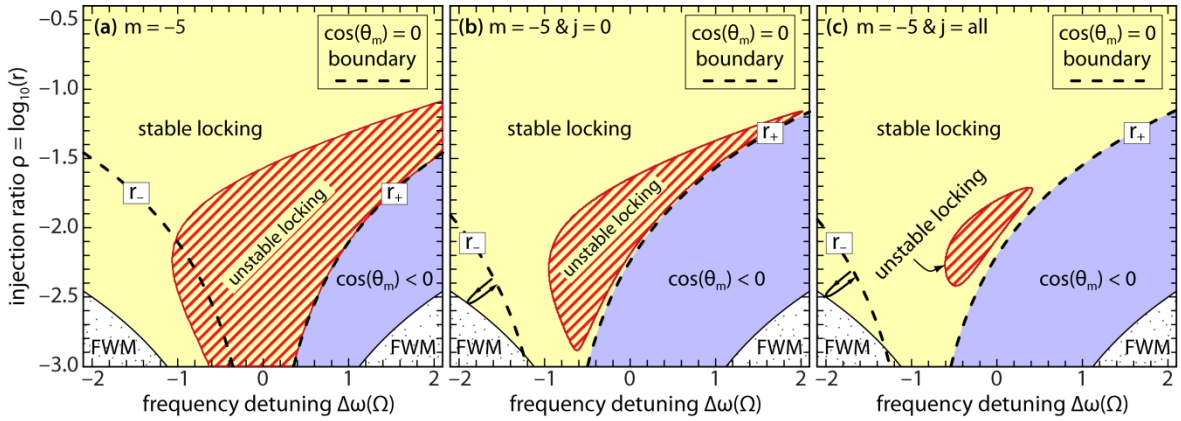

Fig. 1. Stability map for n_L. (a) injection into the side mode m = -5, and no other modes taken into account (b) injection into m = -5, with one other (central j = 0) mode included (c) injection into m = -5 with all unlocked modes included. The size of the "unstable locking" region shrinks significantly between the approach used for prior work in the field (a), and our approach (c).

We find that this region is actually comprises two regions: the "unlocking" region, (marked by $\cos(\theta_m) < 0$ in Fig. 1, where θ_m is the phase difference between the free-running and the injection-locked state), and the "unstable locking" region, marked by the hatched area in Fig. 1, in which eigenvalues of the system lie in the right-half of the complex plain. In Fig.1, dashed lines r_- and r_+ are the left and the right locking boundaries, respectively determined by $\cos(\theta_m) = 0$. Taking just one additional unlocked mode into account when generating the stability map [in case of Fig.1(b), the central, dominant mode, $j = 0$], the "unstable locking" region becomes considerably smaller, while in the latter case [Fig.1(c)], in which all unlocked modes are taken into account, this region becomes very small.

As we had previously discussed in [6], for given values of $\Delta\omega$ and S_{inj}, in the presence of the unlocked modes, the function of dn/dt versus n can have up to three steady-state solutions: $n_{sp}^{(1)}$ and $n_{sp}^{(2)}$, which are results of the injection locking,

and $n_{sp}^{(3)}$, which is mainly a consequence of the unlocked modes. The solution n_L which appears in $\Delta\omega$-r space, always maps into $n_{sp}^{(1)}$, while n_H maps either into $n_{sp}^{(2)}$ or $n_{sp}^{(3)}$. Since $n_{sp}^{(2)}$ was shown to be always unstable [6], we focus on the regions where bistability between n_L and $n_H = n_{sp}^{(3)}$ can exist. For $\Delta\omega > -1.13\Omega$, function *dn/dt (n)* has a solitary solution ($n_{sp}^{(1)} = n_L$), and the "unstable locking" hatched region is shown in Fig.1(c). For $\Delta\omega < -1.13\Omega$, the locking range in the $\Delta\omega$-r space is folded down along the FWM boundary [Fig.1(b) and 1(c)], leading to the overlap of the two locking regions in the r-range, between the FWM boundary and r_-. Within the locking range, the FWM boundary becomes irrelevant, since on both of its sides the injection locking is possible. On the inner side of the FWM boundary, the injection locking is in the n_L state, while on the outer side (from FWM boundary to r_- boundary), the injection locking is in the n_H state. The shaded background in Fig. 2(a) represents the region in which n_L maps into $n_{sp}^{(1)}$, left-hatched region stands for $n_H = n_{sp}^{(2)}$, while right-hatched region stands for $n_H = n_{sp}^{(3)}$. In order to have bistability, $n_L = n_{sp}^{(1)}$ and $n_H = n_{sp}^{(3)}$ must be both stable and share the same $\Delta\omega$ and S_{inj}. In Fig. 2(b) we show parts of $n_L = n_{sp}^{(1)}$ and $n_H = n_{sp}^{(3)}$ regions which are stable (filled regions), and although having the different r, share the same S_{inj}, and thus the same *dn*/*dt* curve. In this region of bistability, a hysteresis cycle appears.

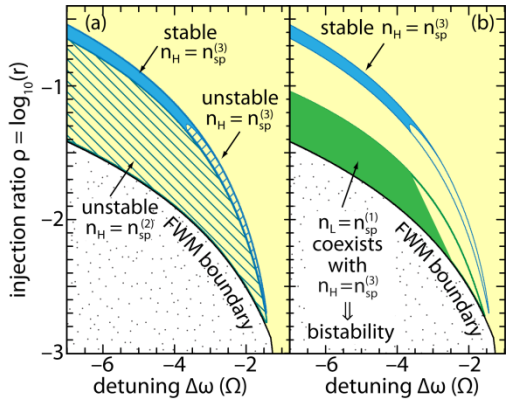

Fig. 2. (a) Stable part of $n_H = n_{sp}^{(3)}$ (filled), unstable $n_H = n_{sp}^{(3)}$ (rigth-hatched), unstable $n_H = n_{sp}^{(2)}$ (left hatched). (b) coexisting bistability regions (dark shaded).

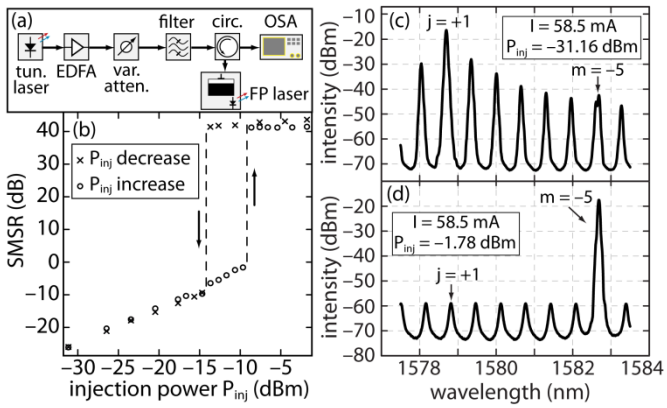

Fig. 3. (a) Experimental setup used for bi-stability characterization; (b) SMSR versus injected power for modes m=-5 and j=+1. Crosses correspond to injected power reduction, and circles to increase; (c), (d) Examples of slave laser output spectra used for data in (b).

The hysteresis and the bistability predicted by our analysis was experimentally investigated using a setup shown in Fig. 3(a). A widely tunable semiconductor laser source was connected to an erbium-doped fiber amplifier, whose output was led to a variable attenuator, and a tunable optical filter. The signal was then coupled into an optical circulator, which was also connected to a Fabry-Perot laser diode chip (FPLD) (through a lensed fiber), and to an optical spectrum analyzer (OSA). Due to the circulator properties, only the signals generated by the FPLD were detected and displayed on the OSA. The FPLD was fabricated at UCSB, in a surface ridge platform [5]. The laser ridge is 500 μm long and 3 μm wide, and the active region consists of an offset quantum well stack, as detailed in, per example, [7]. The insertion loss through the system was characterized by measuring the power through the circulator, and the coupling losses for the laser chip were measured by reverse biasing the laser diode and by measuring the photocurrent generated by the input optical signal of known power.

To characterize the bistability, the side mode suppression ratio between modes m=-5 and j=+1 was measured, and plotted in Fig. 3 (b). The injected signal was in this case detuned by -5Ω. For each value of the injected power, an optical spectrum trace was taken. From it, the SMSR was then calculated. Two spectra, corresponding to two data points from Fig. 3(b) are shown in Fig. 3(c) and (d). Fig. 3(c) corresponds to a low injection case of -31.16 dBm where the laser operates in the multi-longitudinal mode regime, and (d) corresponds to the injection-locked, single mode case, where P_{inj} = -1.78 dBm. The shape and size of the SMSR plot, Fig. 3(b) qualitatively match well the predictions based on our modeling work.

In summary, we have shown that including of all the modes in an injection-locked Fabry-Perot laser considerably modifies the commonly defined locking range map, which is obtained by the analysis of the injection-locked side-mode alone. The folding down of the locking range leads to a multiplicity of the stationary points and consequently to the slave laser bistability, which we have experimentally evaluated and quantified in this work.

[1] J. Ohtsubo, *Semiconductor Lasers: Stability, Instability, Chaos* (Springer-Verlag, Berlin, Germany, 2008).
[2] A. Murakami, IEEE J. Quantum Electron. **39**, 438 (2003).
[3] T. B. Simpson, J. M. Liu, K. F. Huang, and K. Tai, Quantum Semiclass. Opt. **9,** 765 (1997).
[4] T. B. Simpson, Opt. Commun. **215**, 135 (2003).
[5] L. Coldren, S. Corzine, M. Mašanović, *Diode Lasers and Photonic Integrated Circuits*, (Wiley, 2012).
[6] M. M. Krstić, J. V. Crnjanski, and D. M. Gvozdić, IEEE J. Selected Topics Quantum. Electron. **18**, 826 (2012).
[7] M. L. Mašanović et. al., IEEE J. of Lightwave Technology, **23**, 1350 (2005).